Candidate number: 289452
Word Count: 6653

MPhys Project
University of Oxford

AO13: Instrument to sample and return airborne particles from an unmanned aerial vehicle

Supervisors- Dr A. Povey, Dr D. Peters and Prof R. Grainger

April 25, 2015

Abstract

The aim of this project was to install an electrostatic precipitator (ESP) in an unmanned aerial vehicle (UAV) for the purpose of collecting tropospheric aerosol particles. To enable installation it was necessary to rewrite the code used by the ESP to make it possible to activate the ESP remotely. Physical alterations to the layout of the ESP were made to allow it to fit inside the UAV body. Having made these modifications, a size distribution of aerosol particles produced using the ESP was then compared against a distribution produced by a Scanning Mobility Particle Sizer Spectrometer (SMPS) in a laboratory experiment. Quartz particles were dispersed with N_2 and passed through both instruments. The best sample taken by the ESP was imaged using a scanning electron microscope (SEM) and image analysis software used to determine the size distribution of the imaged particles. This distribution was found to broadly agree with the distribution from the SMPS for particle diameters greater than 0.2 μm. At smaller particle diameters software artefacts prevented the smallest quartz particles from being resolved. Following comparison to the size distributions of common aerosol particles found in the literature, it was concluded that limitations in the ability of the ESP to resolve particles less than 0.2 μm would not prevent it from obtaining useful size distributions in fieldwork. Finally, a plan for conducting test flights with the ESP installed in the UAV is discussed.

1 Introduction

Aerosols are liquid or solid particles in suspension in the atmosphere, the study of which is of great importance in the field of atmospheric physics. Aerosols have a key effect on climate: they are the nuclei about which water vapour condenses to form cloud droplets and they contribute to the planet's albedo through their scattering of light and absorption of solar and long range radiation [1]. Consequently, atmospheric aerosols have an important role in determining the precipitation rates and lifetimes of clouds. Common aerosol types include salt from breaking waves, Saharan dust and carbon particles and sulphates from anthropogenic sources such as biomass burning and industry. Another source of aerosols of particular interest to environmental scientists is volcanoes. No two eruptions are identical [2]; the plume of ash released during an eruption is unique. In situ samples of the size and number distributions of ash particles can be combined with satellite data to model the evolution of the ash cloud. This modelling is used to determine no-fly areas, a relatively recent example of which was imposed during the eruption of Eyjafjallajökull in 2010. Improved modelling of the ash cloud could potentially reduce disruption to air traffic. Taking samples from a volcanic ash cloud is a task for which a UAV is ideally suited. In general, data collection using UAVs is cheaper and faster than using an aeroplane as preparation times are short and little manpower is needed [3]. In the case of an ash cloud, UAV data collection is safer too as the UAV can be used to collect data from regions of the cloud where pilots would be reluctant or forbidden to fly.

Despite their importance in the climate system, relatively little is known about the exact spatial distribution of atmospheric aerosols. An example of the uncertainty surrounding these distributions is AERONET, a globally distributed network of sun-photometers which compare measurements of direct solar radiation to expected measurements in order to determine

the aerosol optical depth in the atmosphere at each location [4]. This method makes the assumption of a homogenous, idealised aerosol and so provides column averages for the volume of air measured which isn't necessarily physically representative [5]. There is value then, in conducting in situ measurements of type and size of aerosol to validate satellite and AERONET retrievals. In March 2006, a group from the University of San Diego experimented in creating vertical aerosol profiles above the Indian Ocean using instruments mounted in UAVs. The group found that the profile based on UAV data was 'consistently lower' than the AERONET profile with a mean bias of 19%. The reasons for these differences were attributed to the assumptions made in the AERONET algorithm but also to the existence of aerosols above the UAV flight ceiling of 3km and the presence of gases such as NO_2 which absorb in the visible spectrum and so reduce the radiance measured by the UAV's onboard photometers [6]. Clearly then, this is an area in which further study would be of value, especially if the UAVs used carried instruments other than photometers to allow a more precise determination of the effect the assumptions of AERONET have on the vertical particle distribution produced. This project is concerned with fitting an electrostatic precipitator (ESP) inside a UAV in order that the UAV may be used to take samples of atmospheric aerosols. The ESP has been built by previous MPhys students to the specifications for a handheld ESP in Miller et al [7].

2 Background

2.1 The electrostatic precipitator (ESP)

The principle of operation of an ESP is to collect aerosol particles on a scanning electron microscope (SEM) grid by generating a strong electric field between a needle and a grounded, metallic, SEM grid substrate (see figure 1). The high density of field lines near the tip of the anode needle results in corona discharge. The ionised air particles then drift towards the substrate grid and transfer a charge to aerosol particles carried in a laminar flow of air that is drawn through the instrument. The newly ioinsed aerosol particles drift onto the SEM grid substrate at a rate determined by their mobility in the electric field. The particular ESP used in the project

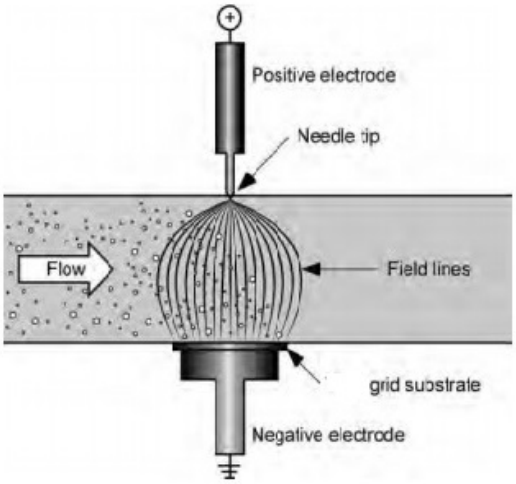

Figure 1: The principle of operation of the ESP- aerosol particles carried by the flow of air through the instrument become ionised and follow the fieldlines of the very strong electric field running between needle and substrate, ultimately becoming deposited on the substrate. [7].

had three such needles and deposition substrates which could have a high voltage applied across them in sequence. Henceforth, the metallic substrate used for SEM viewing will be referred to as a 'SEM pin' or 'pin'. Note that there is an upper limit to the magnitude of the potential used. If the potential difference exceeds $V_{Breakdown}$, then the resistance of air drops dramatically and arcing occurs which scorches the substrate. This is represented by the dotted line in figure 2. $V_{Breakdown}$ is given by:

$$V_{Breakdown} = \epsilon d, \tag{1}$$

where ϵ is the dielectric strength of dry air ($3\text{x}10^6\,\text{V m}^{-1}$) and d is the distance between needle and substrate. In the case of the ESP in question $d \approx 5\,\text{mm}$, giving a maximum potential of 15 kV. In fact the ESP is limited to operating at 5.5 kV, just above the 'corona threshold' (the minimum voltage needed to produce corona discharge). Miller et al found by testing their prototype ESP that an unstable corona region exists at around 6.5 kV and upwards (see figure 2) in which current randomly fluctuates due to the gap between the needle and substrate acting as a variable resistor. The resistance of the gap varyings according to environmental factors such as temerpature and humidity, in addition to ion concentration. The fluctuating current in this region reduces the collection efficiency [7].

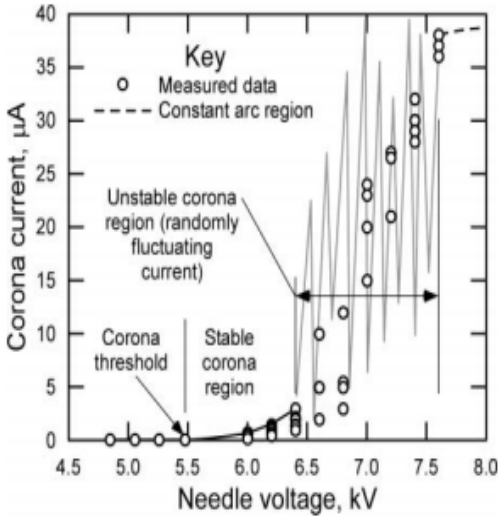

Figure 2: A plot of current versus voltage illustrating the corona threshold at 5.5 kV, above which aerosol particles will become ioinsed and can consequently be collected and the unstable corona region above ∼6.5 kV. In this region, the needle current fluctuates greatly, which leads to inefficient sampling [7].

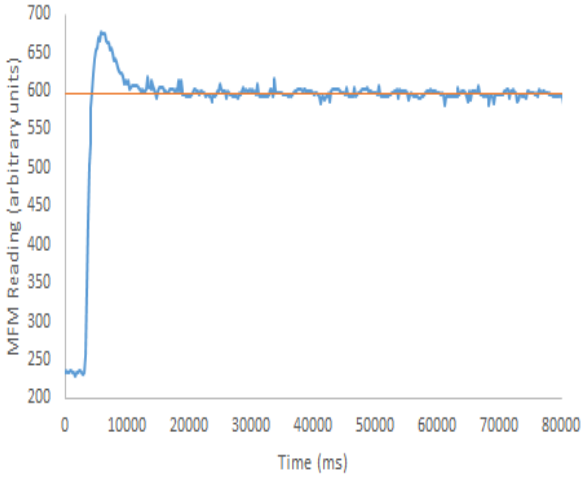

Figure 3: Mass flow Meter (MFM) measurements showing oscillations in the pump flow. The target or 'setpoint' was set to 597 (55 ml min^{-1}) at 12537 ms and is represented by the orange line. Note the initial 'overshoot' due to the PID control loop overcompensating for the flow rate being so far below the target when the setpoint is initially raised.

A pump is used to draw air through the instrument to produce a flow of 55 ml min^{-1} between needle and substrate. The pump is controlled by a PID (proportional-integral-differential) loop which uses the deviation of the current flow rate from the target flow rate to correct the pump's output to make it as close to the target flow rate as possible. This method of control will lead to narrow oscillations about the desired 'setpoint' but considerable overshoot when initially trying to obtain this (see figure 3). When the 'setpoint' is raised to 55 ml min^{-1} from 0 a large negative error is introduced which produces a large positive error due to the integrated term in the control loop, producing an overshoot. For this reason, when the pump is activated in flight a period of around 30 seconds must be left for the oscillations in pump flow to settle before sampling should begin.

2.2 The UAV

Previous iterations of this project had intended to mount the ESP in a Quest 300, however, for logistical reasons the slightly smaller training version, the Quest 100, was chosen. Although the Quest 100 holds a smaller payload, it was possible for the purposes of a test flight to fit the ESP if the autopilot was removed and the UAV flown manually with the aid of the on board 'co-pilot'. The 'co-pilot' is a horizon sensor which aids the operator in keeping the craft level.

3 ESP installation in the UAV

3.1 Software development

An arduino UNO board was used as the microcontroller for the ESP and could be programmed in the arduino language, a variation of C++. For previous projects, Dr Peters had written a code which used serial port communication between a laptop and the arduino board to allow control of the ESP through keyboard commands. For the purposes of laboratory testing the use of keyboard commands to activate and deactivate the pump and high voltage supplies and to set parameters such as pump speed and needle voltage was sufficient. However, for installation in the UAV it was necessary to adapt the old code for the instrument to accept both keyboard commands and a servo signal as inputs. A servo signal is a square wave which may have the widths of its peaks adjusted by remote control. Use of the servo enabled the UAV operator control over the timing of sampling during flight. This is important in enabling the ESP to meet the research aims of the project as sampling can begin when the UAV is ideally positioned. For instance, in the case of sampling volcanic ash, the UAV could

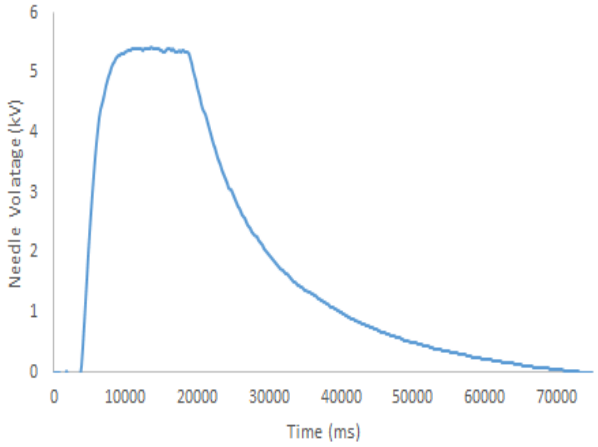

Figure 4: Measurements of needle voltage with time: the timescale for discharge is much greater than that for charging.

enter and exit the ash cloud once for each pin and sampling be timed to begin as soon as the UAV enters the cloud to enable the effectiveness of the collection period to be maximised. It was found that the arduino and ESP could be powered in flight directly from the UAV's on-board battery without needing to use a voltage regulator.

The program written averaged over five servos cycles at a time and turned on the pump when the average length of the peak was below a critical value of 1500ms. This was to prevent noise in the servo signal from activating the ESP prematurely. After waiting for 30 seconds for the flow through the pump to stabilise (see figure 3) a voltage would be applied to the needles to enable aerosol collection. After this time, the pump would remain on for 60 seconds whilst the needle voltage discharged. As can be seen in figure 4 the timescale for discharge is around 50s; it is necessary to keep a flow of air over the substrate to try to limit aerosol particles from depositing on top of one another. It is important to prevent this from happening as the SEM will be unable to resolve the individual particles and so the size distribution produced will not be of good quality.

Another element of the new code was the storage of data in the (EEPROM) internal memory area of the arduino board. It is desirable to have a record of the mean voltage and pump flow to ensure that firstly, the ESP actually turned on (the loading of the SEM pins is very light, so there is no visible change in the top surface after sampling) and secondly, that the instrument performed as expected during sampling. The rate of pumping through the ESP is very slight and can easily be disrupted by vibrations ($\oint$5.1). If estimations of aerosol number densities are to be made based on the size distributions collected, then the volume of air that passed through the ESP must be accurately known. The EEPROM memory area is small, containing only 1024 Bytes[8], so it was not possible to save every reading. Two subroutines were written: the first added the readings from the current iteration of the program's main loop to those already saved in the EEPROM memory and saved the updated number in the same location. As these numbers were long integers, it was necessary to split each one into its constituent bytes, which were then saved individually. Providing that a voltage was being applied across at least one of the needles, this subroutine would continue to save readings in this way with each iteration of the main loop. Using exactly the same method, the subroutine also saved the number of iterations the loop had been through since activation to enable a rough mean to be calculated. The function of the second subroutine was to retrieve the data stored in the EEPROM, recombine the stored bytes and divide the total of the mass flow/voltage measurements by the number of iterations to give a rough mean. As mentioned previously, in flight the board was powered by the UAV's internal battery. It was important to ensure that power fluctuation in the UAV's battery which could turn the arduino board off and on again would not affect the order of needle activations. To this end, the number of activations since launching was saved in the EEPROM. The value of this integer was used as a condition for activating the high voltage supplies, thus preserving the order of the needle activations.

3.2 Physical installation

To physically install the ESP in the UAV it was necessary to a make a number of changes to the instrument. Firstly, the two 500ml reservoirs used by the pump were replaced by two emptied freezer packs of approximate volume 440ml to enable the reservoirs to fit in the body of the UAV. The only significant effect on pump oscillations was to increase the period of the initial overshoot, so the program was modified to leave 60s between the pump turning on and the beginning of sampling. Secondly, it was necessary to house the mass flow meter, pump and pump filters on top of the Perspex cover that protects the high voltage needles to compact the ESP to

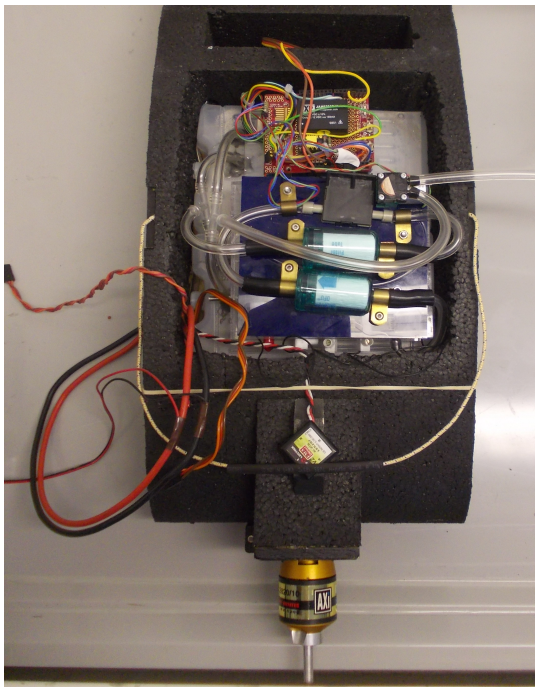

Figure 5: The ESP installed inside the body of the UAV.

allow it to fit within the body of the UAV along with the control systems for the UAV. A hole large enough for the ESP was simply cut into the polystyrene body of the UAV and the ESP and control systems inserted, as seen in figure 5. As can be seen in figure 15, standoffs were added to the stack of boards to protect the connectors from damage in the case of a hard landing.

3.3 Super-isokinetic sampling and Inlet design

Isokinetic sampling refers to where there is no change to the speed and direction of airflow upon entering an inlet [9]. From this definition, the inlet diameter, d, needed for isokinetic flow can be found by equating the volume of air entering the inlet per second to the flow rate through the ESP itself, f:

$$\frac{\pi d^2}{4}\bar{v} = f, \tag{2}$$

where $\bar{v}$ is the mean air speed of the UAV. Taking $\bar{v}$ to be $27\,\mathrm{ms}^{-1}$ and the pump flow rate to be $55\,\mathrm{ml\,min}^{-1}$ gave an inlet diameter of $0.25\,\mathrm{mm}$. The trial inlet used in this case was a conical glue dispenser nozzle attached to a Luer Lock Connector of inner diameter $0.21\,\mathrm{mm}$. Using a diameter smaller than that necessary for isokinetic sampling ensures that the average velocity of the UAV will be within the super-isokinetic sampling regime. In this regime streamlines are bent towards the inlet, as illustrated in figure 6. The effect of this on airborne particles is determined by their modified Stokes number, defined as:

$$stk_{\mathrm{mod}} = \frac{2a^2\bar{v}\rho}{9\eta d}, \tag{3}$$

where a is the particle radius, ρ the particle density and η the dynamic viscosity of air. The dependence of the modified Stokes number on a^2 means that small particles such as the aerosols we wish to study will be disturbed greatly by the bending of streamlines while larger particles will be undisturbed. Super-isokinetic sampling therefore preferentially samples smaller aerosol particles at the expense of larger particles [11] to maximise the collection efficiency.

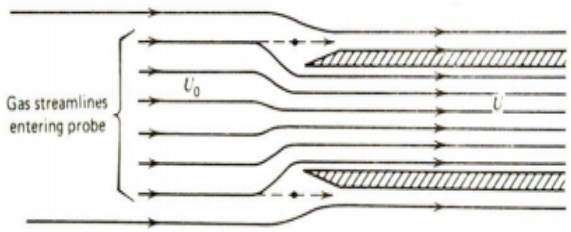

Figure 6: A depiction of super-isokinetic sampling [10].

A hole was drilled in the front of the body of the UAV to allow the inlet to be positioned as seen in figure 7. The intention of this positioning is to maintain laminar flow through the ESP by sampling air beyond the boundary layer of the UAV. The tubing connecting the ESP housing to the inlet was kept as straight as possible to minimise losses. Note that a trade-off exists between improved sampling by projecting the inlet further from the body of the UAV and safety in the case of a crash (one of the advantages of the rear mounted propeller of the UAV is that it reduces the chance of injury were the UAV to hit a bystander).

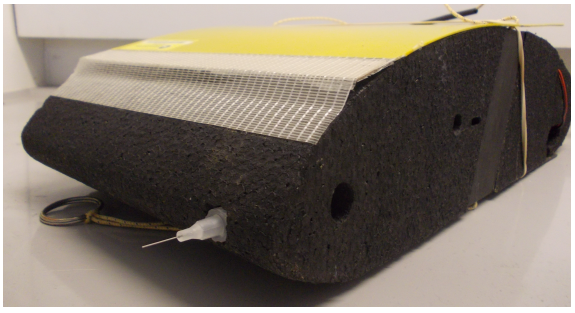

Figure 7: A view of the trial inlet.

Evaluating the efficiency of this inlet was beyond the scope of this project (a BA project existed to help design an optimised inlet [12]), however, rearranging equation 3 can give an estimate of the maximum particle size for a particle to be virtually unaffected by superisokinetic sampling. For instance, taking $\rho = 1\,\mathrm{kg\,m^{-3}}$; $\eta = 1.8\mathrm{x}10^{-3}\,\mathrm{kg\,ms^{-1}}$ [13]; $d = 0.21\,\mathrm{mm}$ and $\bar{v} \approx 27\,\mathrm{ms^{-1}}$ one finds $a \approx 80\,\mu\mathrm{m}$ when 0.1 is taken as the modified Stokes number below which particles are not subject to any inertial separation process [11]. The aerosol particles that are of interest for collection in the ESP have radii on the order of 1 μm [14] so theoretically the inlet design should not have a significant effect on the performance of the ESP.

4 Calibration of the ESP

Having made the necessary changes to the software and hardware of the instrument to enable it to fit inside and be operated from a UAV, a couple of land-based experiments had to be conducted before it was ready for flight.

4.1 Optical regime

One of the aims of installing the ESP inside a UAV is to take in situ measurements of aerosols which can validate and improve satellite retrievals. Previous projects have conducted lab-based experiments with the ESP using artificially high aerosol concentrations. An obvious question to ask then is whether the ESP can produce stubs suitable for SEM analysis in ambient air within the flight time of the UAV. Running the ESP on the roof of the AOPP building for a 15 minute exposure time produced the pin seen in figure 8. A pin that has patterns of deposition that can be clearly viewed under an optical microscope is highly overloaded for the purposes of SEM imaging. An ideal pin for SEM analysis will consequently be one in which no aerosol deposition can be distinguished by the optical microscope, so the exposure time of the ESP in flight will be significantly shorter than 15 minutes. Typical flight times for the Quest UAVs are on the order of 1 hour [15], so there is more than enough time to expose three pins for sufficient lengths of time to be viewed using the SEM.

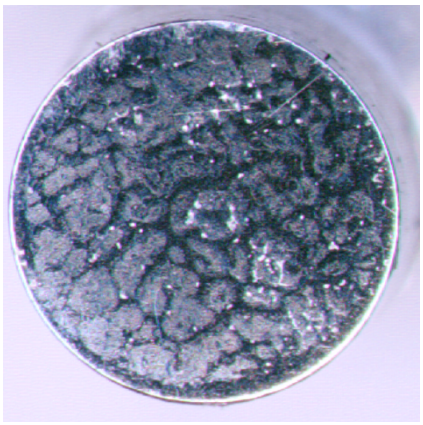

Figure 8: Optical microscope image of a pin exposed to ambient air for 15 minutes.

4.2 Comparison of ESP with OPS and SMPS data

Work was done at the Molecular Spectroscopy Facility (MSF) at the Rutherford-Appleton Lab (RAL). A Phd student was using a number of instruments, including: an Optical Particle Counter (OPC), a Scanning Mobility Particle Sizer Spectrometer (SMPS) and an Aerodynamic Particle Sizer (APS) in order to obtain size distributions for a number of mineral aerosols. The aim was to compare the size distribution produced by SEM analysis of the pins in the ESP with those produced by these instruments in order to further understanding of how the ESP performs when studying realistic aerosol concentrations. A powdered sample of quartz (SiO_2) was injected into an aerosol cell using a EEMS Wright Dust Feed (eWDF). The aerosol cell featured an upwards travelling turbulent jet flow to ensure that the injected aerosol was well mixed with N_2 which was also injected into the cell. After approximately twenty minutes a sufficient concentration of aerosol had accumulated and was considered sufficiently well mixed to sample. Valves were opened to allow flow through the OPC, SMPS and APS. Thirty minutes later, a valve was opened to allow flow through the ESP. Opening this valve caused considerable disruption to the flow through the entire system. The system's exhaust was a fume cupboard, however, opening the valve to the ESP could cause back drafting through the system as the exhaust was pressurised. This in turn could introduce ambient aerosols into the system, which would affect the quality of the data collected. Running the ESP towards the end of the sampling period meant that better data

would be collected from the other instruments but then the ESP risked collecting an insufficient number of aerosols for SEM analysis as the number density of SiO_2 in the aerosol cell became depleted. For reference, a diagram illustrating the experimental setup is included in the appendix, see figure 16.

Once the ESP had been exposed to the flow two pins were taken: one was exposed for six seconds and the other for sixty. A third pin was left in the ESP unexposed during that time to act as a control. The valve was then closed again and the pump stopped while the pins were changed. Following the same procedure, a pin was then exposed for ten minutes and another pin left in the ESP as a control. These order-of-magnitude steps in exposure time were taken because, as mentioned previously, the exposure time needed to produce a pin with sufficient loading to allow a representative size distribution to be created without being so overloaded that aerosol particles deposited inhomogeneously was unknown. The pins had to be handled delicately with tweezers during the process of removing them from the ESP to prevent scratching and contamination through contact with skin. Nevertheless, ambient aerosols were still present in the SEM image. Whether these aerosols were deposited when the pins were exposed to ambient air during the pin changing process or had already been deposited on the tungsten needle during previous experiments is unclear. Replacing these tungsten needles, a difficult task as it requires disassembly of the ESP housing, is perhaps a wise precaution to take before further investigations are carried out with the ESP.

4.2.1 SEM analysis

The pins were subsequently viewed using a SEM. It was found that the pins that were exposed for 6s and 60s had not collected significantly more particles than the control. The pin exposed for 600 seconds had collected enough quartz particles to perform image analysis on. Figure 9 gives an example of a SEM image of the pin. The white particles are quartz whilst the dark particles are impurities which as discussed above, could have been introduced when the pin was exposed to ambient air during the pin removal process. The scratches visible are artefacts from the polishing process used to clean the pins.

The size distribution seen in figure 10 was produced using imageJ, a program for image analysis. The program enables the user to subtract the image background in order to automatically determine the area of particles present. Note that particles were assumed to be perfect spheres. This analysis was carried out on the clearest 12 SEM images. Unfortunately the program cannot completely remove the background from the image. The result is that artefacts, typically less than 5 pixels in area, which could be scratches or other aerosols which have settled on the pin during the removal process, are counted as part of the distribution. The expected peak of the distribution is around 300nm, however, the 'noise' from this process leads to a very sharp peak around 200nm. It is difficult to determine the extent to which noise has contributed to this peak. A possible route around this in future would be to take SEM images at much greater magnifications such as x3500[1] in order to better resolve the smallest particles. However, as SEM time is very restricted and expensive, this would mean that fewer quartz particles could be imaged, leading to a less representative distribution.

The distribution produced from analysis of the pins taken from the ESP was compared to the distribution taken from the SMPS spectrometer. The SMPS spectrometer was chosen for comparison because its range of measurement of the diameters of airborne particles (between 2.5 nm and 1 μm) includes the expected peak of the distribution [16]. Figure 10 shows the two distributions plotted on the same axis. For particle diameters greater than 0.2 μm there is a good agreement between the SSMPS distribution and the normalised ESP distribution. However, the effect of 'noise' in the image has clearly had a dramatic impact on the SEM distribution for diameters less than 0.2 μm. As mentioned previously, future studies could aim to take more images at a higher magnification to provide better resolution of the lower portion of the distribution. However, should these studies be under the same time constraints with the SEM or suffer from aliasing[2] of small particles at greater magnifications. It would be worthwhile to consider what effect this limit on resolution could have on obtaining representative distributions during fieldwork.

Table 1 contains a list of common aerosols and a lower and upper bound for the diameter of a typical particle. These are based on the approxi-

[1] A magnification of x2000 was used to take figure 9

[2] The edges of particles appearing jagged

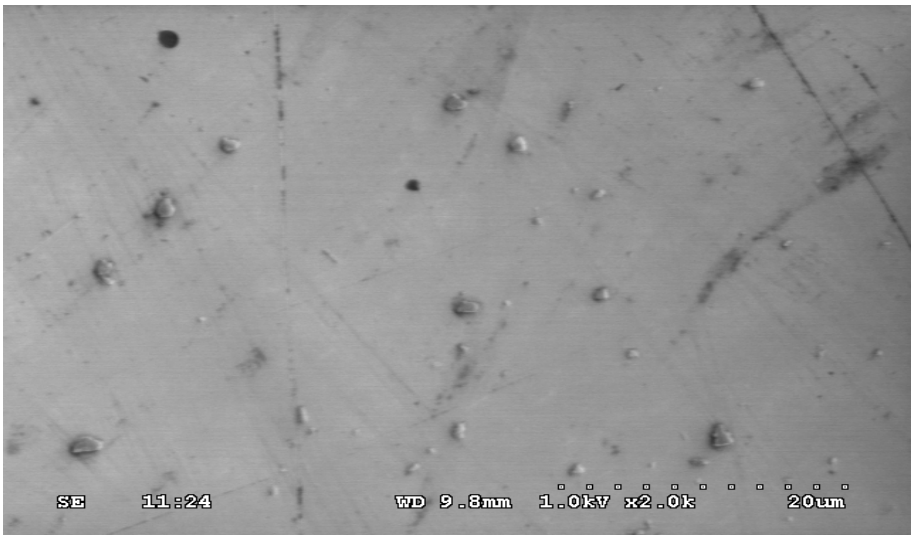

Figure 9: SEM image of the pin that was exposed for 600 seconds. The grey particles are quartz (SiO_2), while the dark particles are assumed to be ambient aerosols which have been inadvertently collected. Note the dark lines which are scratches that are artefacts from the polishing proccess used to clean the pins before use in the ESP.

mate full width half maxima of the size distributions given in the Optical Properties of Aerosols and Clouds (OPAC) model [18]. Based on this data, we would expect the ESP to struggle to resolve the majority of water-soluble aerosols such as sulphates and fine sea salt and mineral particles. For the purposes of validating AERONET retrievals this is arguably unimportant as larger particles will have a greater scattering cross section and make more of a contribution to the scattering albedo. For the purpose of analysis of volcanic ash, the data suggests that the ESP should not have a problem in resolving the size distribution. However, note that a significant number of volcanic ash particles will have diameters greater than the limit of 80μm which was calculated as the maximum diameter for a particle to be unaffected by super-isokinetic sampling ($\oint$ 3.3). It may well be the case that the sampling bias of the inlet prevents good reolsution of the upper part of the distribution. The calculation made in section 3.3 is only a rough one, so further study as described in section 5.2 would be needed to determine whether this is a serious limitation.

Aerosol	d_{lower} (μm)	d_{upper} (μm)
Mineral (fine)	0.02	0.4
Mineral (coagulated)	1.2	8
Insoluble (e.g. soil)	0.2	4
Water soluble (e.g. sulphate)	0.05	0.4
Sea salt (fine)	0.16	1.2
Sea salt (coagulated)	0.8	6
Volcanic ash [17]	9	101
Soot	0.01	0.06

Table 1: A table of common aerosols and a range of their diameters based on the full width half maxima of OPAC data.

4.2.2 ESP exposure times

Previous iterations of this project used the following equation to provide a rough guide for calculating pin exposure times:

$$\tau_{exposure} = \frac{{r^2}_{pin}}{nQ{r^2}_m}\left[\frac{L}{100}\right], \qquad (4)$$

where r_{pin} is the pin radius, L the loading of the pin as a percentage, r_m is the average aerosol radius, n is the aerosol number density and Q the flow rate through the ESP. This equation makes a number of assumptions, the most significant of which being homogenous deposition and a collection efficiency of 100%. The previous iteration of this project studied patterns of deposition at

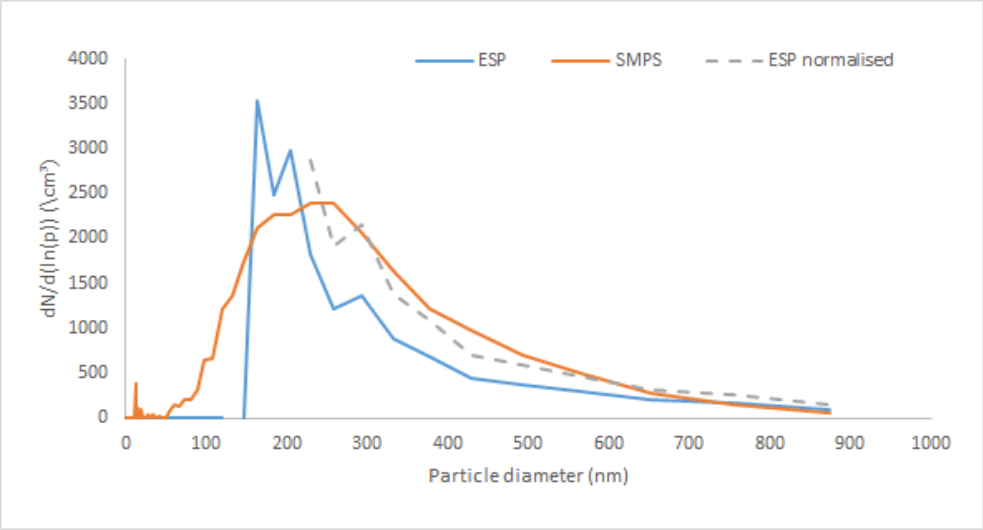

Figure 10: A size distribution based on software analysis of a sample taken using the ESP (blue line) is plotted on the same axes as another distribution based on an independent measurement made by the SMPS (orange line). The grey line is a replot of the ESP data which has been normalised and had the lower size bins removed, showing good agreement with the SMPS distribution.

high loadings[3] and found that they were highly inhomogeneous. It was difficult to determine whether this was due to defects in the sharpness and orientation of the tungsten high voltage needles or was a result of the behaviour of the soot particles being studied [14]. It was certainly noticeable when studying a much lower loading of SiO_2 that there was much greater deposition in the centre of the pin, which would support the hypothesis that it is the needles themselves which contribute to inhomogeneous deposition.

To quantify the ESP collection efficiency it would be necessary to calculate the loading of the SEM images and multiply by the flow rate and exposure time to give a number density which could be compared n. This problem is probably not worth studying however, as the inlet design will in isolation contribute its own inefficiencies which will affect sampling times. Once the ESP is flying in the UAV regularly, a better understanding of the necessary exposure times will most likely grow as more samples are taken.

5 Further Work

5.1 Alterations to the ESP

Prior to any test flights, a useful test would be to remove the propeller of the UAV but run the motor whilst on the ground to confirm that the vibrations of the aircraft do not significantly affect the PID control of the pump. It was found whilst testing at RAL that pump oscillations were significantly affected when the ESP was left on a vibrating surface. Should the vibrations of the craft prove to have little effect on the pump rate then the ESP could be considered ready for a test flight in its current configuration in the Quest 100. If there is sufficient time before the test flight it may well be worth reconsidering the use of the freezer packs as reservoirs in any case. The pipes connecting the packs to the instrument were simply glued in place which was expedient but meant that there was always the risk of air leakage, especially if they were handled roughly (as may well be the case in flight). Attaching the pipes to a fitting, or to a metal plate that was glued inside the packs would be a better method of attachment. Even better would be to custom make a new pair of reservoirs out of Perspex or some other sturdy plastic, perhaps using a 3D printer. These reservoirs would thus retain the flat shape which is advantageous when fitting the ESP inside the body of the UAV but be less prone to puncture or acting like a diaphragm when vibrated by the UAV.

As mentioned in Section 4.2, it would perhaps be a wise precaution to clean or replace the tungsten needles in the ESP to ensure that no aerosols can be transferred from the needles to the pin before the ESP is used for further experiments. However, as was found by the previous

[3] 40-50% loading- a much lower covering of particles is required to ensure that the SEM can image individual particles

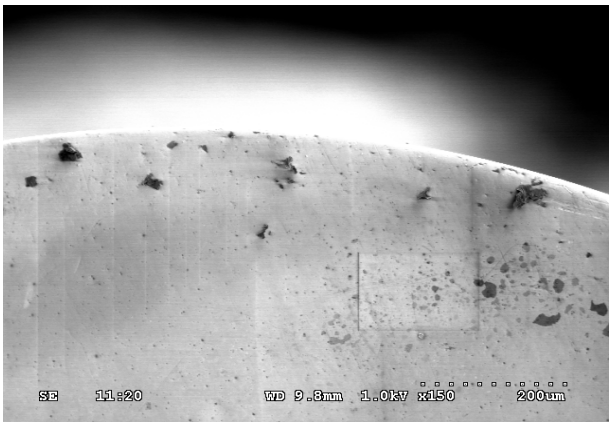

Figure 11: SEM image of the edge of one of the pins- note the rectangular area which has been degraded by the SEM.

student [14] the IPA used for cleaning degrades the pins which can lead to an inhomogeneous pattern of deposition. Now that the ESP is so close to being flight-ready it would perhaps be a sensible idea to replace the needles so that the instrument can be used to respond quickly to any potential eruptions. Some consideration could also perhaps be given to the method of removing the pins from the ESP. A rubber 'O' ring ensures that there is an airtight seal between the inserted pin and the ESP housing, however, the rings also make it difficult to remove the pins. The large dark particles visible in figure 11 have likely been deposited there during the struggle to remove the pin from the ESP. The useable area of the pin for analysis is restricted by this. For now, this is not the most important improvement that needs to be made. That being said, as can be seen from the rectangular pattern visible towards the right side of figure 11, the SEM degrades the portion of the pin it is viewing and so portions of the pin can be 'lost' for imaging purely in trying to focus the SEM. In addition, it was fortunate that the SiO_2 particles used in this project's experiment were very different in appearance to these particles. Future studies of larger aerosol particles may not be so lucky and could well study aerosols which appear similar to the smaller black particles found towards the bottom left of figure 11. Reducing the deposition of unwanted aerosol could be important in preventing needless confusion.

5.2 Test flight

Assuming the vibrations of the UAV do not affect the performance of the pump unduly, the ESP is now in a position where it is ready to be flown in a UAV. However, further work must be done before it can be considered ready for use in the field, mounted in the UAV. As previously mentioned, a tangential BA project designed an optimised inlet for use in the UAV. A first step would be to manufacture this inlet and then conduct a test flight to investigate whether ignoring inefficiencies due to the sampling inlet as I have done in this project is a valid assumption ($\oint$3.3). This could be done by comparing the size distributions of three pins that were exposed whilst airborne (probably using order of magnitude-differing exposure lengths again i.e. 6, 60 and 600 seconds) against those of pins that were taken whilst the UAV was stationary on the ground. The UAV would have to be flown low in order to minimise differences in aerosol concentrations due to altitude. Ideally, the result of this trial flight would be that superisokinetic sampling using the optimised inlet has little effect on the collection efficiency of the ESP. Should this prove not to be the case, then further thought will have to be given to the inlet design. An alternative experiment that could allow greater control over the UAV's environment would be to place the body in the UAV in a subsonic wind tunnel. Two pins could be exposed for the same length of time: one when the UAV body is orientated so that the inlet is pointed directly into the flow to simulate flight and the second with the UAV body reversed so that $\bar{v} \approx 0$ but the aerosol concentration in the ambient air remains the same. This setup would enable testing of a variety of inlets at differing values of $\bar{v}$. Better understanding of how airspeed affects the quality of the sampling would be helpful in designing flightplans that optimised collection. For instance, in the case of taking samples from a plume of volcanic ash, deciding between a slower, spiralling flight path along the edges of the plume or a number of faster 'passes' which cut across the periphery of the plume. Dispersing and then injecting a sample of volcanic ash into the wind tunnel would also help determine whether the sampling bias of the inlet in super-isokinetic samping affects the ESP from resolving the upper part of the volcanic ash distribution- a potential issue that was raised in section 4.2.1.

5.3 Alternative plumbing arrangement

Should a Quest 300 body become available, then a filter holder could be installed in the UAV in addition to the ESP. A Y-splitter would be inserted after the inlet and a second pump used to draw air through the filter assembly at a rate of $1\,\mathrm{ltr\,min^{-1}}$. The filter would be weighed before and after the flight and as the flow rate through the filter is known this would give an estimate of the aerosol density. Comparison of this value to PM 2.5 data would provide another way of testing the efficiency of the inlet and would certainly be easier than having to use the SEM and then imageJ to obtain size distributions. The code written for this project has already been modified to allow for PID control of two pumps but it would also be necessary to upgrade the size of the arduino microcontroller from an Arduino Uno to an Arduino Mega to provide enough digital pins for control.

6 Conclusion

The ESP is now closer to being flight ready than it has ever been. Three major steps have been taken during this project to bring the ESP to this position:

- Code was written for the arduino microcontroller which enabled remote activation of the ESP through the use of a servo signal.
- The reservoirs used by the ESP's pump were replaced and the layout of the ESP's components altered significantly so that the ESP could be accomodated inside the body of the UAV. Also, standoffs were added between the circuit boards of the ESP to prevent damage to the connectors between the boards in the case of a crash landing.
- Comparison was made between a size distribution produced using the ESP to one from a SMPS. There was found to be good agreement between the two instruments for particle diameters greater than $0.2\,\mu$m (see figure 10). This is reassuring given that the aerosols that the ESP will be used to study in the field will be larger than this in general (see Table 1).

In particular, the work done on comparing the ESP to the SMPS was useful as it gave an idea of the limitations of the ESP's resolution. The ratio of this limit of resolution to the scale (pixels/micron) of the SEM image will likely hold at other magnifications, so could prove a useful guide to deciding what SEM magnification to use in the future. As SEM time is so constrained, choosing the right magnification which can be used to image as many deposited particles as possible in the time available but be of sufficient resolution for the imageJ software to distinguish them is very important. The goal of the project was to modify the ESP to the state where it could be installed in a UAV and dispatched quickly to the scene of a volcanic eruption or could be used in field studies to validate AERONET retrievals. However, before it can be claimed that this target has been met, a test flight as discussed in section 5.2 is an essential piece of further work which must be carried out to ensure that the inefficiencies of the ESP inlet does not significantly effect the quality of sampling. Unfortunately, logistical and safety concerns meant that it was not possible to carry out the test flight within the period of this project[4]. Nevertheless, the work conducted during this project will be a valuable stepping stone to making the ESP fully flight ready and eventually conducting exciting and useful research.

[4]There is a maximum wind speed of 20 knots beyond which it becomes too difficult to fly the UAV. In addition, a spotter with a licence to fly the UAV as well as an operator are required for safety

Acknowledgements

Gratitude must be extended to Drs Povey and Peters, my immediate supervisors, for their invaluable help and guidance. Also, I wish to thank Jon Temple and Wayne Tubby for their help in modifying the ESP; Paul Pattinson for cheerfully teaching me how to use the SEM and Ben Reed for sharing his experimental setup and results with me whilst I was at RAL.

References

[1] F.W. Taylor, *Elementary Climate Physicsl*, 1st edition, Oxford University Press, 2005.

[2] H.R. Shaw, *Uniqueness of volcanic systems*, Geological Survey Professional Paper, Volumes 2, 1358-1394, 1987.

[3] NASA, *UAV Auntonomous Operations for Airborne Science Missions* http://ti.arc.gov/m/profile/frank/aiaa_wegener.pdf.

[4] O. Dubovik, P. King, *A flexible inversion algorithm for retrieval of aerosol optical properties from Sun and sky radiance measurements*, Journal of Geophysical Research-Atmospheres, Vol. 105: 20673-20696.

[5] NASA, *AERONET Inversion Products* http://aeronet.gsfc.nasa.gov/new_web/Documents/Inversion_products_V2.pdf. Last acessed 27/03/15.

[6] C.E. Corrigan, G.C. Roberts, M.V. Ramana, D. Kim and V. Ramanathan, *Capturing vertical profiles of aerosols and black carbon over the Indian Ocean using autonomous umanned aerial vehicles*, Atmospheric Chemistry and Physics, 8, 737-7470, 2008.

[7] A. Miller, *A handheld electrostatic precipitator for sampling airborne particles and nanoparticles*, American Industrial Hygiene Association 25, 8-24, 1964.

[8] Arduino, *EEPROM* http://arduino.cc/en/Reference/EEPROM. Last acessed 25/03/15.

[9] W.C. Hinds,*Aerosol Technology: Properties, Behaviour and Measurement of Airborne Particles*, 2nd edition, Wiley-Interscience, 1999.

[10] F. Drewnick, *Physics and Chemistry of Aerosols, Chapter 6, Measurement techniques 1* http://www.mpic.de/fileadmin/user_upload/pdf/Dokumente_Schneider/Lecture/Drewnick_Aerosol_2013_-_Chapter_6__Measurement_Techniques_1.pdf. Last acessed 26/03/15.

[11] M. Wendisch, J.L. Brenguier, *Airborne Measurements for Environmental Research* 1st edition, Wiley, 2013.

[12] BA group, *TIP_06: Nozzle design for a UAV experiment*, 2015.

[13] L.D. Landau, E.M. Lifshitz, *Fluid Mechanics*, 2nd edition, Pergamon Press, 1987.

[14] A. Thawer, *AO11- Instrument to sample and return airborne particles from an unmanned aerial vehicle* MPhys project, 2014.

[15] QUEST UAV, *Drone Comparisons* http://www.questuav.com/news/drone-comparisons. Last acessed 25/03/15.

[16] L.S. Ruzer, N.H. Harley, *Aerosols Handbook: Measurement, Dosimetry and Health Effects*, 2nd edition, CRC Press, 2013

[17] C.J. Horwell, *Grain-size analysis of volcanic ash for the rapid assessment of respiratory health hazard*, Journal of Environmental Monitoring 9: 11071115, 2007.

[18] M. Hess, P. Koepke and I. Schult, *Optical Properties of Aerosols and Clouds: The Software Package OPAC*, Bulletin of the American Meteorological Society Vol. 79, No. 5: 831-844, 1998.

7 Appendices

7.1 Additional ESP photos

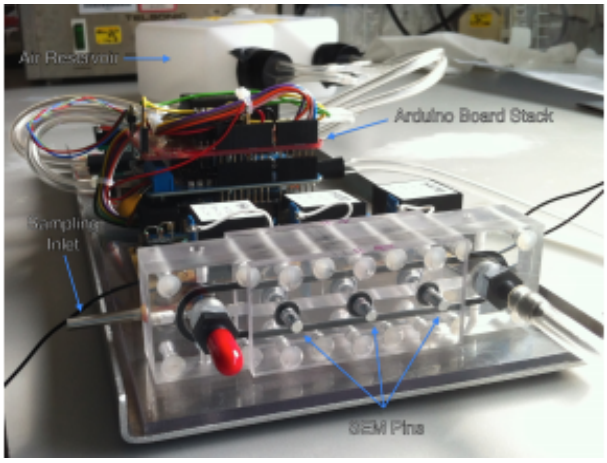

Figure 12: Side-on view of the ESP before modification [14].

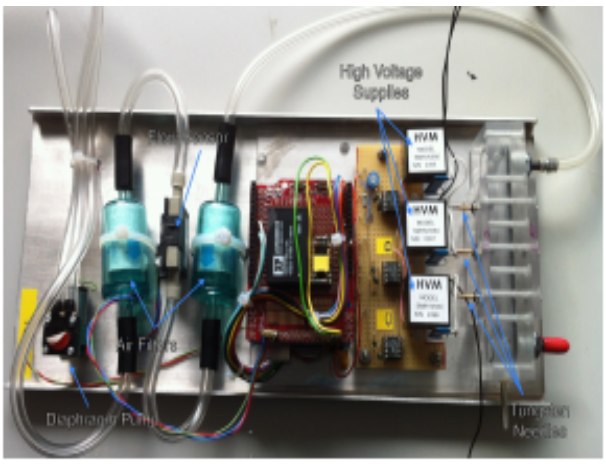

Figure 13: Top-down view of the ESP before modification [14].

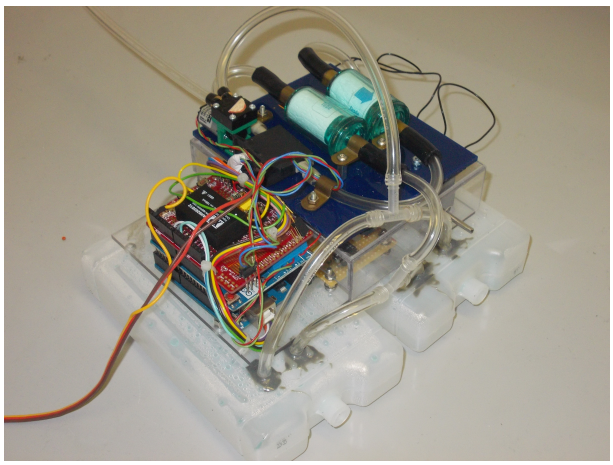

Figure 14: The ESP modified for installation in the UAV.

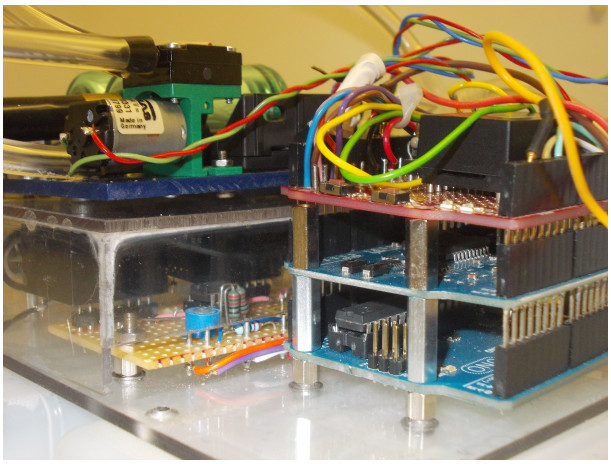

Figure 15: View of the arduino boards, showing the new standoffs.

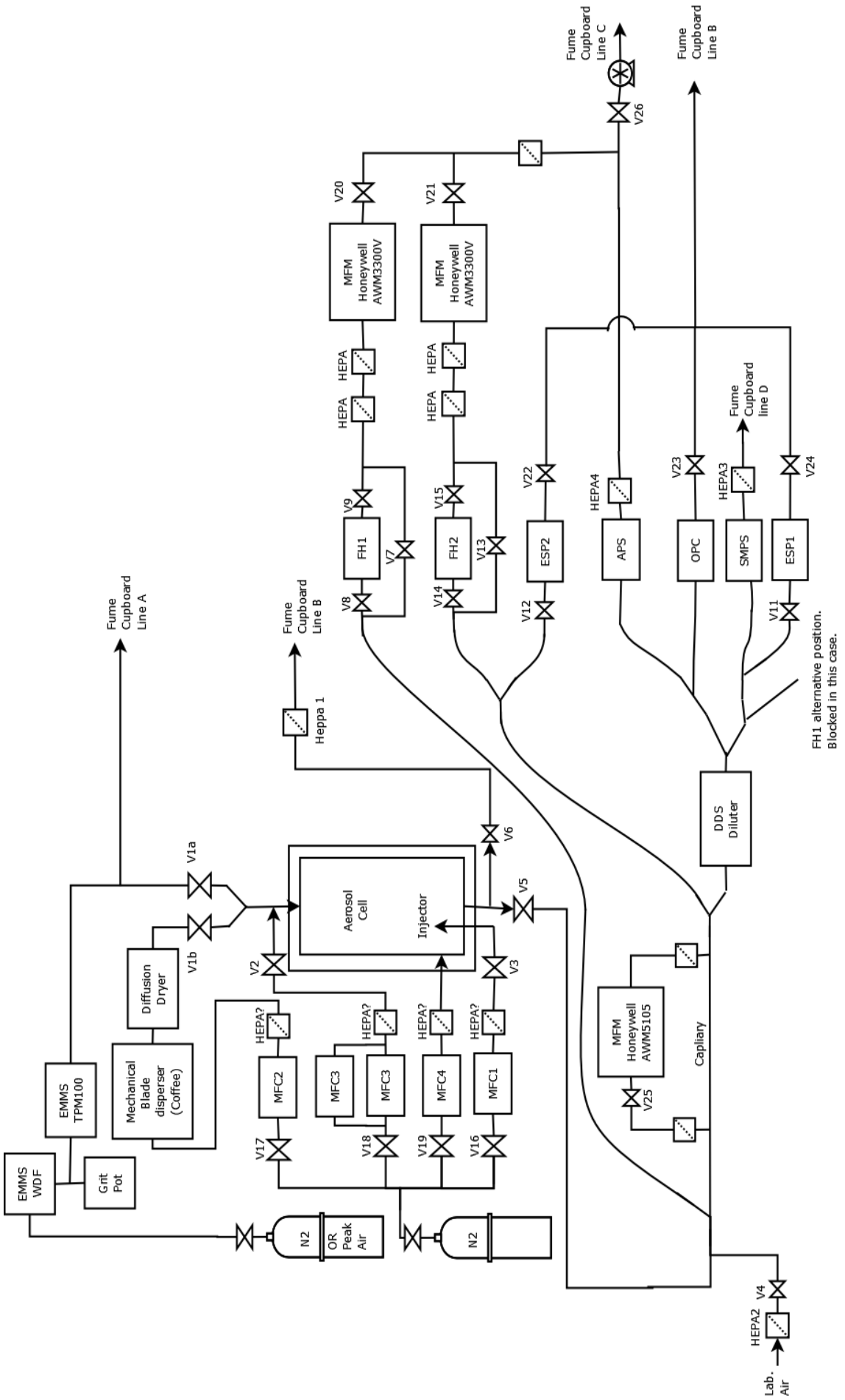

Figure 16: Diagram showing the plumbing of the setup at RAL- the ESP was placed in the location for 'ESP1'.